Structure of the {001} talc surface as seen by atomic force microscopy: comparison with X-ray and electron diffraction results

Eric FERRAGE[1],*, Grégory SEINE[2], Anne-Claire GAILLOT[3], Sabine PETIT[4], Philippe DE PARSEVAL[5], Alain BOUDET[2], Bruno LANSON[6], Jocelyne FERRET[7] and François MARTIN[8]

[1]Department of Mineralogy, The Natural History Museum, Cromwell Road, London, SW7 5BD, UK
[2]CEMES, UPR 8011 CNRS, 29 rue Jeanne Marvig, F-31055 Toulouse Cedex 4, France
[3]Department of Earth and Planetary Sciences, Johns Hopkins University, 34 and N. Charles streets,
Baltimore MD 21218, USA
[4]HydrASA, UMR 6532 CNRS-Université de Poitiers, 40 avenue du Recteur Pineau, F-86022 Poitiers Cedex, France
[5]LMTG, UMR 5563 CNRS-Université Paul Sabatier-IRD, Observatoire Midi-Pyrénées, 14 avenue Edouard Belin,
F-31400 Toulouse, France
[6]Environmental Geochemistry Group, LGIT, UMR 5559 CNRS-Université Joseph Fourier, BP53,
F-38041 Grenoble Cedex 9, France
[7]Talc de Luzenac S.A., BP 1162, F-31036 Toulouse Cedex, France
[8]LASEH, HydrASA, UMR 6532 CNRS-Université de Limoges, 123 avenue Albert Thomas, F-87000 Limoges, France

Abstract: The surface structure of a centimetre sized crystal of talc from the Trimouns deposit (Ariège, France) was imaged by atomic force microscopy. The direct image shows detailed characteristics of clay tetrahedral surfaces. The unit-cell dimensions obtained using atomic force microscopy ($a_{or} = 5.47 \pm 0.28$ and $b_{or} = 9.48 \pm 0.28$ Å) are found to be slightly higher, with a higher uncertainty, than those obtained using X-ray diffraction ($a_{or} = 5.288 \pm 0.007$ and $b_{or} = 9.159 \pm 0.010$ Å) and selected-area electron diffraction ($a_{or} = 5.32 \pm 0.03$ and $b_{or} = 9.22 \pm 0.05$ Å). Talc has a quasi-ideal surface, free from strong structural distortion, as compared to most other clay minerals, and is unlikely to have surface relaxation. The observation, on the obtained image, of apparent cell-dimension enlargement is then more likely attributed to instrumental artefacts, also responsible for scattered values of unit-cell parameters, rather than related to any surface structural features. The interpretation of apparent changes in unit-cell dimensions in terms of structural features for other clay minerals, in which such structural deformations is common (micas, kaolinites and chlorites), should therefore be done with extreme care.

Key-words: talc, atomic-force microscopy, surface structure, X-ray diffraction, selected-area electron diffraction.

1. Introduction

Because of its beneficial properties to manufactured products, talc is widely used in paper coating, paint, ceramics, and polymer industries. In the automotive industry, talc is added to polymers to stabilize and harden automobile spare parts such as fenders, dashboards, steering wheels, *etc*. However, because different talc varieties can exhibit a wide range of physical and chemical properties it is necessary to optimize the use of these different types of talc for specific industrial applications. In particular, it is necessary to take into account the surface structure of talc which, for example, may or may not allow the epitaxial growth of polymers (Ferrage *et al*., 2002).

Over the last decade, the availability of atomic force microscopes (AFM) has provided new insights into mineral reactivity by providing images of crystal growth or dissolution at the micro-to-nanometre scale (Hillner *et al.*, 1992a and b; Kuwahara *et al.*, 1998, 2001; Bosbach *et al.*, 2000; Lindgren, 2000; Bickmore *et al.*, 2001; Brandt *et al.*, 2003; Tournassat *et al.*, 2003; Aldushin *et al.*, 2004; Yokoyama *et al.*, 2005). The AFM has also allowed the direct visualization of the outer surfaces of minerals by imaging either groups of atoms at the molecular scale (Drake *et al.*, 1989; Weisenhorn *et al.*, 1990; Hartman *et al.*, 1990; Johnson *et al.*, 1991; Drake & Hellmann, 1991; Wicks *et al.*, 1992, 1993, 1998; Vrdoljak *et al.*, 1994; Kuwahara, 1999, 2001) or individual atoms (Lindgreen *et*
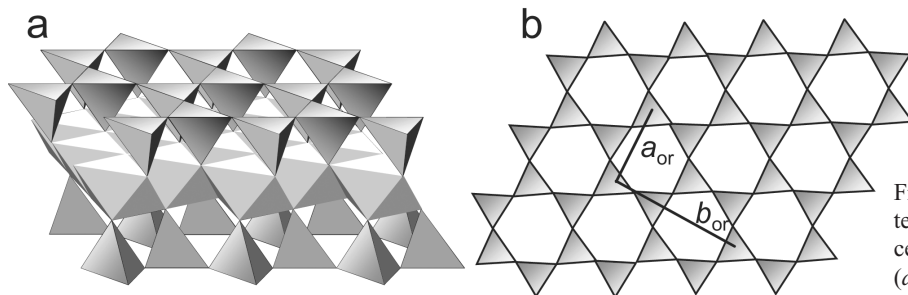
Fig. 1. Talc structure along c^* (a) and the tetrahedral surface plane where the a and b cell parameters in a quasi-orthogonal system (a_{or}, b_{or}) are indicated (b).

al., 1991; Wicks et al., 1992; Vrdoljak et al., 1994; Sokolov et al., 1997, 1999). Because of their perfect cleavage along the {001} plane, which produces extremely flat external surfaces, phyllosilicates are especially well-suited for an AFM study.

The structure of talc differs from that of mica, chlorite or lizardite which were previously imaged by AFM (Hartman et al., 1990; Wicks et al., 1992, 1993, 1998; Vrdoljak et al., 1994; Kuwahara, 1999, 2001; Lindgreen et al., 1991). Talc structure presents two similar external tetrahedral faces, which is suitable for microscopic observations. In addition, the excess of octahedral charges is compensated for by deficiency in tetrahedral charges (Martin et al., 1999), and the 2:1 sheet remains neutral, the interlayer of talc being thus devoid of cations. Finally, the weak substitution in talc layers induce moderate structural distortions such as tilts or tetrahedral rotations.

In this article we report the first atomic force microscope images of the surface of a talc sample composed of very well-stacked layers, from the Trimouns deposit (Ariège, France). Images of the talc surface obtained from traditional AFM in repulsive mode are compared with data in the literature and structural parameters of the bulk structure obtained from X-ray diffraction (XRD) and selected-area electron diffraction (SAED).

2. Background

2.1. Geological setting and sampling

Talc (2:1 layer silicate) has a composition close to that of the $[Mg_3Si_4O_{10}(OH)_2]$ end-member but with minor amounts of Fe, Al and F, and traces of Mn, Ti, Cr, Ni, Na and K (Heller-Kallai & Rozenson, 1981; Noack et al., 1986; Abercrombie et al., 1987; Aramu et al., 1989; Coey et al., 1991; de Parseval et al., 1991, 1993; Martin et al., 1996, 1999). The sample comes from the Trimouns talc and chlorite deposit, located in the French Pyrénées, ~ 100 km south of Toulouse, at an altitude of 1,700 m. The origin of talc is well-established and is the result of the hydrothermal alteration of wallrock in a zone of intense shearing between the Saint Barthélémy basement dome and the low-grade Paleozoic metamorphic cover (Fortuné et al., 1980; Moine et al., 1982, 1989; de Parseval et al., 1993). Dolostones of the Paleozoic cover were transformed to talc, whereas the more siliceous and aluminous rocks (micaschists and granitic pegmatites) evolved to a chlorite-dominated ore

characterized by well-defined metasomatic zones. The sampled talc consists of centimetric flakes, a quality that is commonly referred to as "talc flower" when mined; it was formed within geodes in the dolomite hanging wall of the ore body and is associated with REE minerals (de Parseval et al., 1997).

2.2. Crystallographic data

Talc is a 2:1 phyllosilicate structure (Fig. 1a) with two Si tetrahedral sheets (forming an array of hexagonal rings of SiO₄ tetrahedra – Fig. 1b) each linked through the apical oxygen to form a sheet of octahedrally coordinated Mg^{2+} cations. Early structural characterizations of talc have described its structure as monoclinic ($C2/c$ space group) (Gruner, 1934), but later publications have described it as triclinic ($C\bar{1}$ space group) (Rayner & Brown, 1973) or as pseudomonoclinic (Cc) but using a $P\bar{1}$ space group (Perdikatsis & Burzlaff, 1981). In comparison to aluminous phyllosilicates, the misfit in lateral dimensions between tetrahedral and octahedral sheets is smaller, leading to a better accommodation of the two sheets. As a result, the tetrahedral rotation angle is diminished from ~ 13-14° for muscovite to ~ 3-4° for talc (Radoslovitch, 1961, 1962). The tetrahedral tilt angle out of the basal oxygen plane is very weak, giving an essentially flat {001} surface. The moderate tetrahedral rotations induce a reduction of the SiO₄ ring symmetry from hexagonal into ditrigonal (Fig. 1b).

3. Experimental methods

3.1. Chemical analyses

The chemical composition of the talc sample used in this study was determined using a Cameca SX50 electron microprobe. The sample was imbedded in resin and polished to obtain perfect flat section. Operating conditions were 15 kV and 10 nA with beam size set to 3×3 μm. Standards used for calibration were: wollastonite for Si, corundum for Al, periclase for Mg, haematite for Fe, pyrophanite for Mn and topaze for F.

3.2. X-ray diffraction

To obtain information on the crystallographic parameters, particularly in the ab plane, XRD data was collected

on a randomly oriented sample. The centimetre-sized talc flakes were ground to a fine powder in an agate mortar. XRD data was collected with a Bruker D5000 diffractometer equipped with a Kevex Si(Li) solid-state detector and Cu$K\alpha$ radiation. Intensities were recorded at a 0.02° 2θ interval, from 2 to 90°, using a 50 s counting time per step. Accuracy on 2θ positions was better than 0.001°. A rotating sample holder was used to minimize the effect of preferential orientation. The openings of the divergence slit, the two Soller slits, the antiscatter slit, and the resolution slit were 0.5°, 2.3°, 2.3°, 0.5° and 0.06°, respectively. Cell parameters were refined using U-Fit 1.3 software assuming a $P\bar{1}$ space group (Perdikatsis & Burzlaff, 1981).

3.3. ^{57}Fe Mössbauer spectroscopy

A ^{57}Fe Mössbauer absorption spectrum of the talc was collected over the range ± 4 mm.s^{-1} with a 512 channels analyzer. The Mössbauer spectrometer is composed of a compact detector γ-system for high-counting rates and of a conventional constant-acceleration Mössbauer device (WISSEL). A ^{57}Co (in Rh) source with nominal activity of 50 mCi was used. Talc flakes were finely ground under acetone (to minimize possible oxidation of Fe) and the resulting powder was placed in a plexiglas sample holder. The spectrum was recorded using a Canberra multichannel analyzer at 80 K to benefit from the second-order Doppler effect. The isomer shift was recorded with respect to α-Fe metal. As recommended by Rancourt *et al.* (1992), the absorbtion thickness of the talc sample was calculated to minimize the width of the absorption lines using data from the phlogopite-annite series since phlogopite has a similar Fe-content to that of talc. The values were around 200 mg of mineral per cm². Lorentzian lines shapes were assumed for decomposition, based on least-squares fitting procedures. The χ^2 and misfit values were used to estimate the goodness of fit.

3.4. Selected-area electron diffraction

The electron diffraction study was performed on a Philips 420 transmission electron microscope (TEM) equipped with a tungsten filament and operated at 120 kV. Talc flakes were gently crushed in distilled water and dispersed onto a 3mm holey carbon-coated Cu-mesh TEM grid. Selected-area electron diffraction (SAED) patterns were recorded after orienting talc single crystals along the [001] zone axis using a double-tilt sample holder. The camera constant of the talc SAED patterns was calibrated using a gold reference sample with the crystals oriented along [100]. SAED patterns were recorded under the same parallel beam illumination conditions for both gold and talc samples. The error on the camera constant was estimated to be ~ 0.7 %. Distances between diffraction spots were measured on the negatives using a precision measurement table.

3.5. Atomic force microscopy

The talc surface was investigated by atomic force microscopy (AFM) using a Nanoscope II AFM from Digital Instruments. The talc sample was scanned in air using the repulsive contact mode with constant deflection. The D-head piezoelectric scanner was calibrated using HOP graphite and mica. The pyramidal shaped Si_3N_4 cantilevers from Digital Instrument with 200 μm wide legs and a spring constant of 0.12 N.m^{-1} were used. The talc sample was cleaved along {001} plane surface prior to observation using adhesive tape. Observations were performed using a vibration isolated platform and the thermal drift was minimized by waiting for the AFM to equilibrate with ambient temperature. Contact forces, scan speeds and scan directions were adjusted to optimize the resolution.

4. Results

4.1. Mössbauer spectroscopy

Table 1 lists the iron site-occupancies of the talc spectrum fitting, taking into account the quadrupole splitting distributions (Rancourt, 1994). The spectrum of the talc sample obtained at 80 K (Fig. 2a) is similar to talc spectra reported by Martin *et al.* (1999). It shows a difference in intensity between the two absorption bands, and a significant shoulder on the side of the –0.5 mm.s^{-1} peak. A good fit to the experimental data was obtained with four Lorentzian doublets (Fig. 2b – Table 1). The first two, both with a large quadrupole splitting, are due to Fe^{2+} in octahedral sites. The third doublet with a small quadrupole splitting and a low isomer shift is located within the first absorption band and attributed to Fe^{3+} in the tetrahedral site (Dyar & Burns, 1986; Rancourt *et al.*, 1992; Rancourt, 1993; Martin *et al.*, 1999). The last doublet corresponds to Fe^{3+} in octahedral sites (Blaauw *et al.*, 1980; Dyar & Burns, 1986; Rancourt *et al.*, 1992; Dyar, 1993; Rancourt, 1993; Martin *et al.*, 1999). According to this decomposition, Fe^{3+} cations are thus present in both octahedral and tetrahedral sites. However, Fe^{2+} is the dominant iron species (81 %), thus indicating reducing conditions during the formation of talc.

4.2. Chemical composition

The structural formula of the talc sample was calculated on the basis of eleven oxygens from the average of ten bulk analyses obtained by electron microprobe:
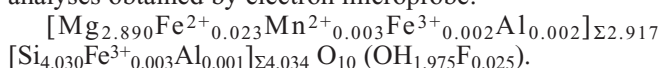
$[Mg_{2.890}Fe^{2+}_{0.023}Mn^{2+}_{0.003}Fe^{3+}_{0.002}Al_{0.002}]_{\Sigma 2.917}$ $[Si_{4.030}Fe^{3+}_{0.003}Al_{0.001}]_{\Sigma 4.034} O_{10} (OH_{1.975}F_{0.025})$.

Table 1. Mössbauer parameters of talc sample at 80 K.

| Fe^{2+} | | | | Fe^{3+} | | | | Fe^{2+} |
δ*	Δ	%	Site	δ*	Δ	%	Site	(Fe^{2+}+Fe^{3+})
1.15	2.85			-0.25	0.21	12	[4]	
		81	[6]					81
1.21	2.96			0.07	0.68	7	[6]	

Note: δ values relative to Fe-metal.

Quadrupole splitting (Δ) and isomer shift (δ) are given in mm.s^{-1}.

Table 2. Comparison of cell parameters.

	a	b	c	α	β	γ	a_{or}	b_{or}
Perdikatsis & Burzlaff (1981)	5.291(3)	5.290(3)	9.460(5)	98.68(5)	85.27(5)	119.90(5)	5.293(4)	9.168(8)
XRD refinement (this study)	5.294(1)	5.281(1)	9.469(1)	98.71(1)	85.11(1)	119.98(1)	5.288(7)	9.159(10)
Electron diffraction (this study)	5.32(3)	-	-	-	-	-	5.32(3)	9.22(5)
AFM (this study)	-	-	-	-	-	-	5.47(28)	9.48(28)

Note: Unit-cell parameters from Perdikatsis & Burzlaff (1981) are transformed to appear in the $C\bar{1}$ space group.

Distances are given in ångströms and angles in degrees. a_{or} and b_{or} represent dimensions of the equivalent C-centred unit-cell with $\gamma_{or} = 90°$).
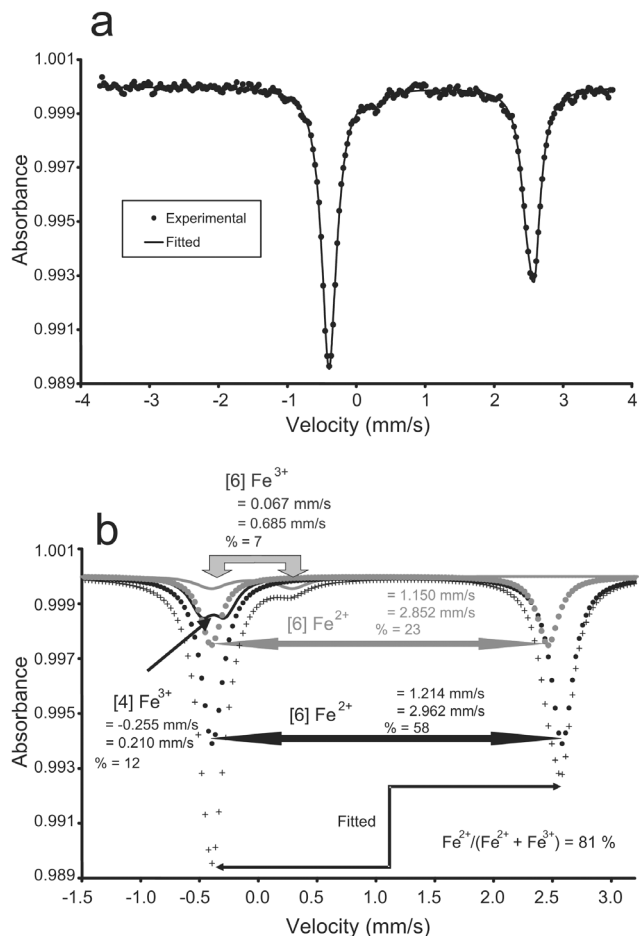

Fig. 2. Experimental and fitted Mössbauer spectrum of talc sample at 80 K (a) and different components of the fitted spectrum (b).
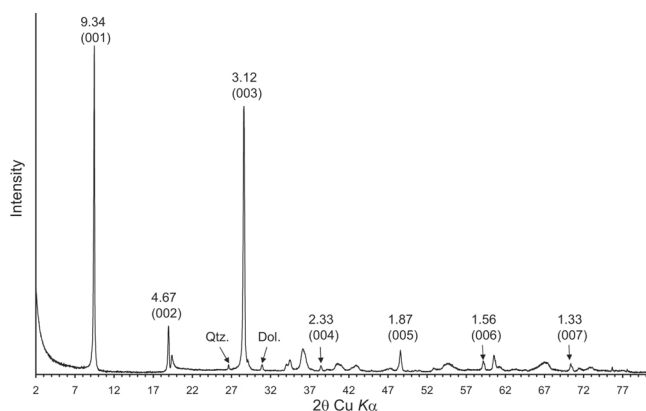

Fig. 3. X-ray-diffraction pattern of talc sample. Dol. and Qtz. represent dolomite and quartz traces, respectively.

The distribution of iron between $^{[6]}Fe^{2+}$, $^{[4]}Fe^{3+}$ and $^{[6]}Fe^{3+}$ was deduced from Mössbauer spectroscopy results. Aluminium was split into $^{[4]}Al$ and $^{[6]}Al$ to insure the neutralization of charges in the octahedral and the tetrahedral sheets, leading to the electroneutrality of the layer. The composition of the talc sample is thus very close to that of the representative talc determined by Martin *et al.* (1999) for the Trimouns deposit. Only minor substitutions are present in the octahedral or tetrahedral sites leading to moderate local distortions in the tetrahedral sheet and thus to a nearly flat {001} surface.

4.3. X-ray diffraction

The powder diffraction pattern of the ground talc powder is characteristic of pure talc with sharp 00ℓ reflections that form a harmonic series ($d_{001} = \ell \times d_{00\ell}$) thus indicating a well-ordered structure along the **c*** axis without interstratification of chlorite layers (Fig. 3). Traces of quartz and dolomite are also detected. Sample unit-cell parameters were refined in the triclinic system ($P\bar{1}$ space group) (Perdikatsis & Burzlaff, 1981) from the positions of all measurable reflections between 2 and 90° 2θ. Unit-cell parameters from the present study are in agreement with those reported by Perdikatsis & Burzlaff (1981) (Table 2). It is possible to deduce the a_{or} and b_{or} dimensions of the usual C-centered pseudo-orthogonal unit cell from the refined *abc* unit-cell parameters defined in the triclinic system (Fig. 1b). As the γ angle is close to 120°, a_{or} is similar to a and b_{or} can be calculated as $b_{or} = a_{or}\sqrt{3}$ (Table 2).

4.4. Selected-area electron diffraction

The SAED pattern of a talc single crystal observed along the [001] zone axis contains very sharp $hk0$ diffraction spots arranged according to a pseudo-hexagonal pattern (Fig. 4). In order to determine unit-cell dimensions in the **a*b*** plane, a_1^*, a_2^* and a_3^* distances were measured along [100], [010] and [110], respectively, and averaged to a single a^* dimension. Measurements were repeated for twelve crystals perfectly aligned along [001], and all values were then averaged to obtain a single a^* unit-cell dimension in the reciprocal space. However, in order to determine the unit-cell dimension in the **ab** plane in the direct space, it is necessary to take into account the 3D symmetry of the unit-cell:

$$a = (\sin\alpha / a^*) / [1 + 2.\cos\alpha.\cos\beta.\cos\gamma - \cos^2\alpha - \cos^2\beta - \cos^2\gamma]^{-2} \qquad (1).$$

As talc crystallizes in a triclinic system, unit-cell dimensions in the direct space cannot be simply deduced from the distances measured on the SAED pattern without making some assumptions for the values of α, β and γ angles. Therefore, α, β and γ values from XRD analysis (Table 2) were used in Eq. 1, and the following relationship was then obtained:

$$a = 1.1545/a^* \qquad (2).$$

Note that the same relationship can be obtained, without using results from XRD, if one assumes that (i) the γ angle is close to 120°, and that (ii) the α and β angles are between 85 and 100° then the approximations $\sin\alpha \sim 1$ and $\cos^2\alpha \sim \cos^2\beta \sim \cos\alpha.\cos\beta \sim 0$ can be used. It follows that from direct measurements of the SAED patterns and from the relation given above (Eq. 2), it is possible to deduce that $a_{or} = a = 5.32(3)$ Å and that $b_{or} = a_{or} \sqrt{3} = 9.22(5)$ Å (Table 2).

4.5. Atomic force microscopy

Micro-topography of cleaved surface

A high-resolution image was recorded to observe the talc surface micro-topography (500×500 nm^2 – Fig. 5). Talc sample exhibits thick crystals in agreement with the macrocrystalline character of the investigated sample. A perpendicular section of talc topography is shown in Fig. 5d and reveals that after cleavage these crystals are several tens of unit layers thick. This sample also has very large domains with flat surfaces which are particularly suitable for AFM imaging. Note the variation in Z direction on these almost flat regions that can be attributed to cantilever vibration, which is greater when recording in air condition than in liquid (Kuwahara *et al.*, 1998, 2001). These regions were chosen for recording molecular-scale image.
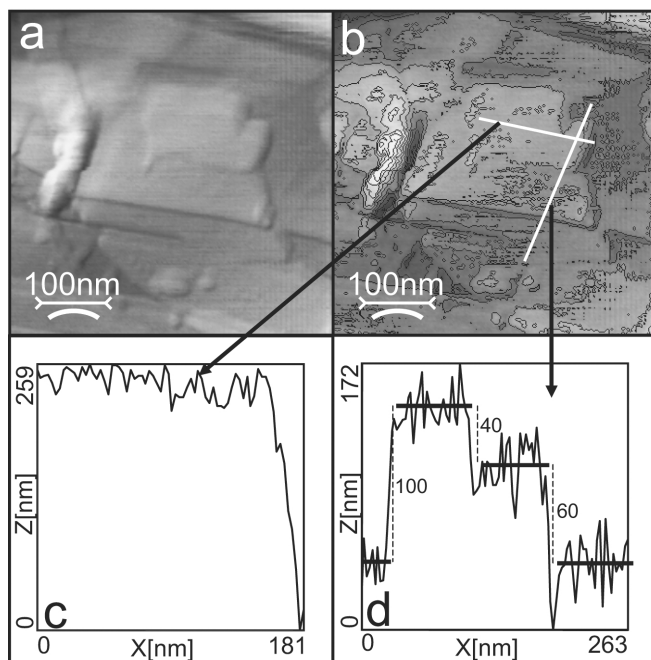

Fig. 5. Micro-topography of talc surface (a) and the same image with isoaltitude curves separated by 70 Å to enhance topography contrasts (b). (c) and (d) represent profiles of cleaved surface morphology.

Molecular scale

The raw image obtained at the molecular scale (5×5 nm^2 – Fig. 6) shows an alignment of triangles on the tetrahedral sheet surface. This raw image can be used to determine the m_i periodicity between adjacent triangles and the
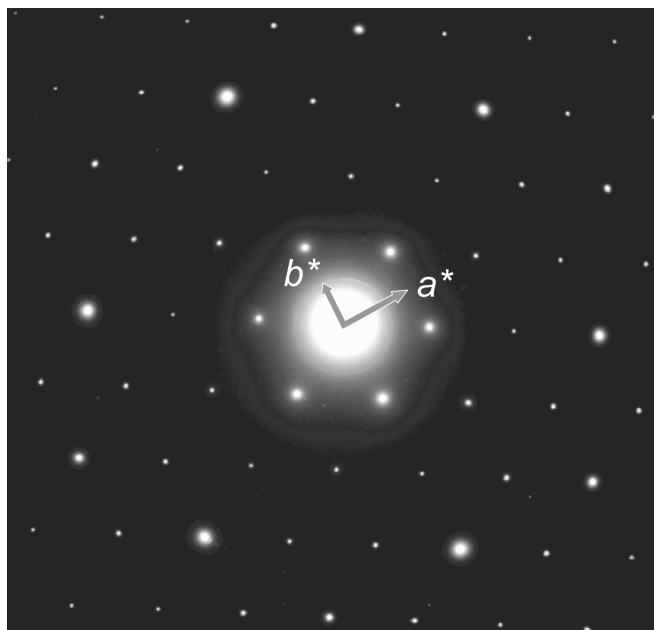

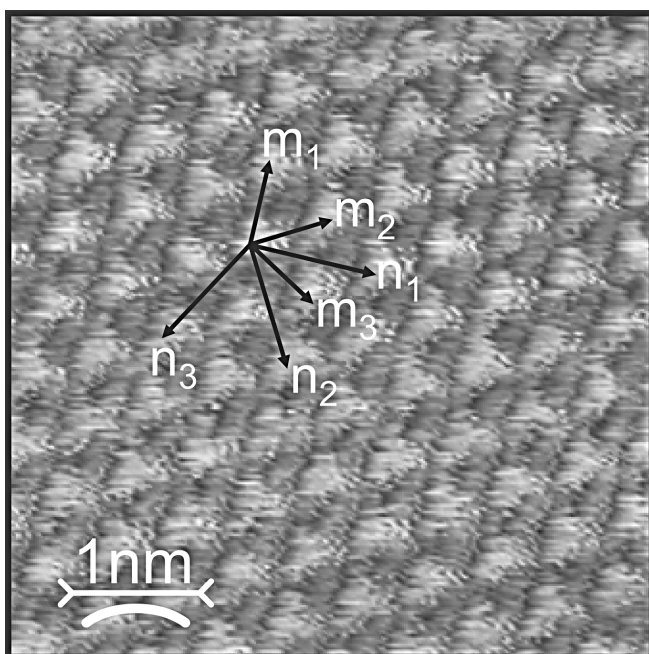Fig. 4. SAED pattern of talc sample recorded along the [001] zone axis.

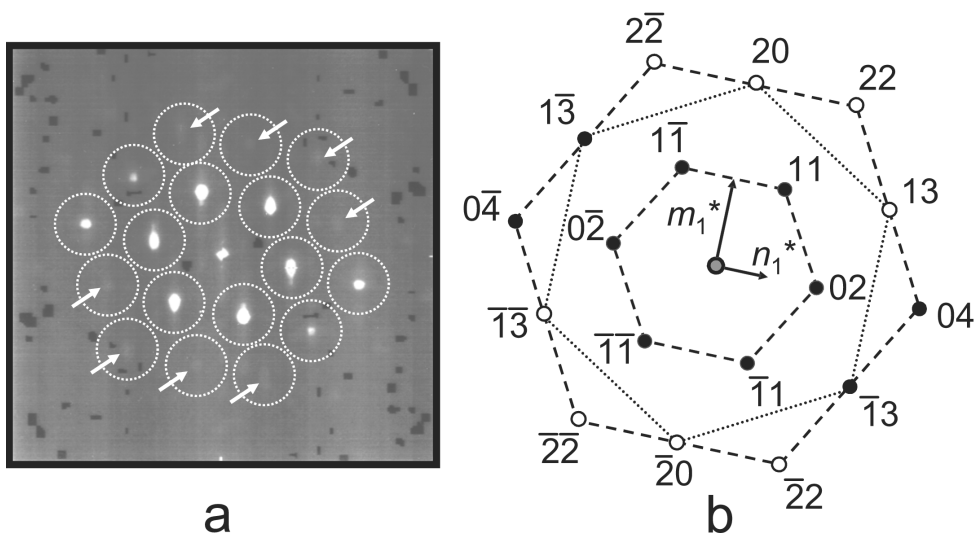Fig. 6. AFM image of talc surface at molecular scale 5×5 nm^2.

Fig. 7. Two-Dimensional Fourier Transform applied to molecular-scale AFM image (Fig. 6 - a) and indexation of spots in reciprocal space (b).
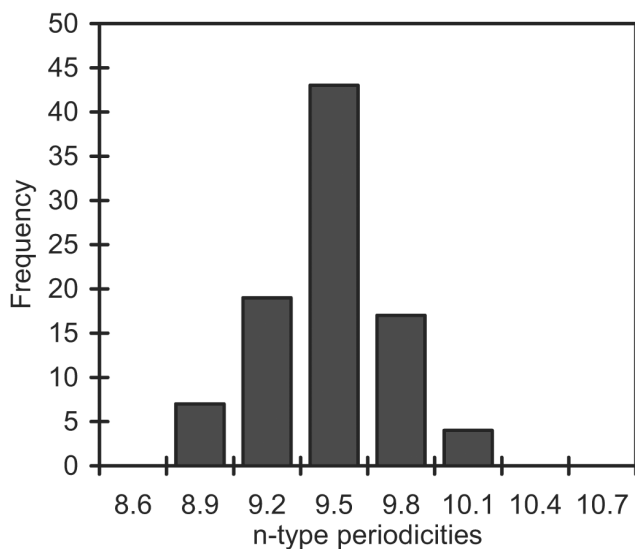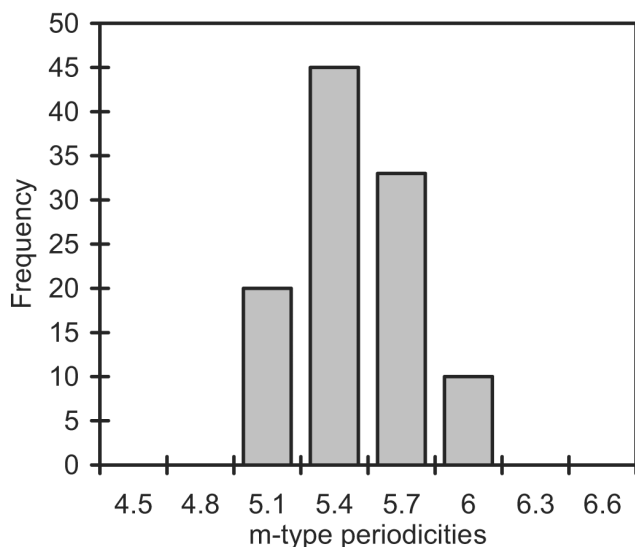

Fig. 8. Histogram of a_{or} and b_{or} cell parameters from AFM molecular-scale image.

n_i periodicities for the second neighbour triangles along the perpendicular direction. Figure 7a shows the two-dimensional (2D) fast Fourier transform (FFT) of the raw image. On this numerical diffraction pattern, spots are distributed according to a pseudo-hexagonal pattern and different orders are visible, which indicate a well-defined periodic surface structure. It is possible to index the spots that correspond to m_i and n_i periodicities along two perpendicular directions in the raw image (Fig. 7b). The regularity of the structure deduced from the sharpness of the diffraction spots on 2D FFT is confirmed by direct periodicity measurements done on the raw image and reported in Fig. 8, and leading to mean values of 5.47 ± 0.28 Å and 9.48 ± 0.28 Å for m_i and n_i periodic distances, respectively.

5. Discussion

5.1 Surface structure of talc

The raw image of talc surface (Fig. 6) is consistent with those found in the wealth of literature devoted to AFM studies of tetrahedral sheet surfaces of phyllosilicates. Some images present an arrangement of hexagonal rings corresponding to the ditrigonal cavities of tetrahedral sheet whereas other images, obtained on micas, show a bright spot periodicity of about 5.1-5.3 Å (which could correspond to the layer unit-cell parameter of most phyllosilicates – Hartman *et al.*, 1990; Lindgreen *et al.*, 1991; Wicks *et al.*, 1992, 1993; Vrdoljak *et al.*, 1994; Kuwahara, 1999, 2001). This periodicity was initially interpreted as the hexagonal array of interlayer cations, but Kuwahara (1999) showed that it was possible to obtain both types of images by varying the scanning angle on the same sample. In addition, basal surface oxygens often display alternating high and low positions for any tetrahedron defining a hexagonal ring. This feature was first interpreted as resulting from the tetrahedral tilt of the basal oxygens, but is now commonly considered to be a topography artefact induced by the interaction between an asymmetric, double-atom, cantilever tip
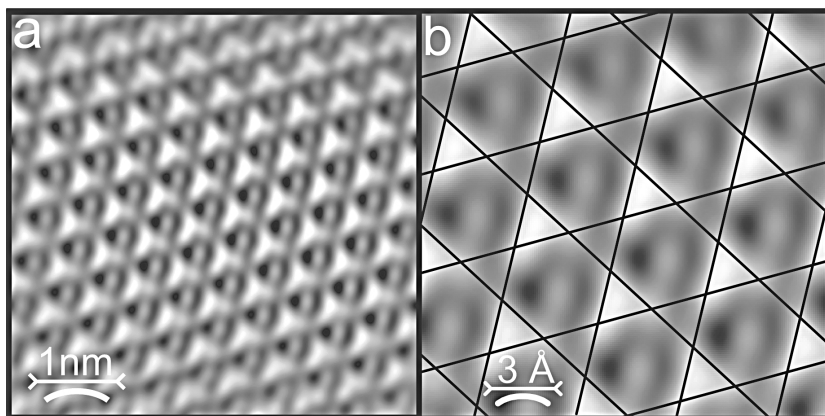
Fig. 9. Image shown in Fig. 5 after application of back 2D FFT to remove extraneous signal (a). An enlarged view of (a) image with a drawing of individual tetrahedra (theoretical tetrahedral rotation not being taken into account - b).

and the surface atoms (Gould *et al.*, 1989; Vrdoljak *et al.*, 1994; Wicks *et al.*, 1998; Kuwahara, 1999, 2001). According to these studies, triangles on the unfiltered image (Fig. 6) represent a height exaggeration of half of a tetrahedra. Thus, m- and n- periodicities between adjacent triangles correspond to a_{or} and b_{or} unit-cell dimensions of talc. Although the AFM image was recorded in air, the image is most likely that of the basal oxygen surface rather than that of some adsorbed species on the talc surface. Such adsorption would indeed result in a blurry image with holes and/or aggregation of these molecules. However, because cantilever drift easily removes interlayer cations from the mica surface, in spite of the strong electrostatic binding forces (Kuwahara, 1999, 2001), a similar "cleaning" of adsorbed species from the uncharged talc surface is most likely to occur.

The 2D FFT in which pseudo-hexagonal pattern was shown with different orders has indicated a well-defined periodic structure (Fig. 7). Back 2D FFT is commonly applied to remove extraneous signal from images, but appears to be a controversial method. The two main criticisms are: i) important features of the raw image are removed and/or features that were not initially present are introduced, and ii) atomic positions are averaged. Wicks *et al.* (1998) discussed thoroughly these potential pitfalls, pointing out that the first point is essentially dependent on the competence of the user who should check carefully the FFT spots. Then, if all the structure information is used in the back 2D FFT operation, only high-frequency noise is removed, and the overall image enhancement does not affect structure details. Wicks *et al.* (1998) also demonstrated that following this image processing, atoms displaced from their ideal positions were not averaged as initially supposed. Figure 9a shows the filtered image from the back 2D FFT of areas outlined on the numerical diffraction pattern (Fig. 7a). The filtered image (Fig. 9a) is essentially similar to the raw image (Fig. 6), but shows a spectacular enhancement of structural features, mainly alternating tetrahedra. The individual positions of tetrahedra can be drawn to reveal the surface structure of talc (Fig. 9b). Note the presence of a small "hump" in the siloxane cavity. However, because of evident artefacts due, in particular, to the interaction between the double-atom cantilever tip and the sample, extreme care should be taken in the interpretation of these features in structural terms.

5.2 Talc unit-cell parameters

To determine the unit-cell dimension of the talc surface layer, approximately 100 measurements in each of the m and n three directions (corresponding to $\mathbf{a_{or}}$ and $\mathbf{b_{or}}$ directions, respectively) were performed on the raw images (Fig. 8). The frequency distribution of m and n indicates a single-mode distribution for each which agrees with published distributions (Vrdoljak *et al.*, 1994; Kuwahara, 1999, 2001).

The a_{or} and b_{or} parameters measured on the talc surface by AFM are 5.47 ± 0.28 Å and 9.48 ± 0.28 Å, respectively (Table 2). The uncertainty is quite high (~ 5 % and 3 % for a_{or} and b_{or}, respectively), but is consistent with other AFM studies on clay minerals (between ~ 2 % and 8 %, *e.g.*, Vrdoljak *et al.*, 1994; Kuwahara, 1999, 2001) regardless of the number of measurements performed on a single image and of the number of images processed. The measured range for a_{or} and b_{or} includes the values expected from the bulk structure determination, although the mean values are high. Similar large unit-cell parameters have been reported for other phyllosilicates, but the uncertainty systematically includes the ideal unit-cell dimensions (Vrdoljak *et al.* (1994) and Kuwahara (1999) on chlorite and muscovite, respectively). This enlargement of unit-cell parameters was attributed to surface relaxation. However, in contrast to micas or chlorite, no interlayer sheet or cation contributes to interlayer cohesion in talc. As a result, surface relaxation is unlikely for talc and the observed variation in unit-cell dimensions may rather be attributed to instrumental effects as evoked by Vrdoljak *et al.* (1994). Note that improved unit-cell dimensions could be obtained by recording images in liquid environment rather than in air conditions as done in the present study (Kuwahara 1999, 2001; Sokolov *et al.*, 1997, 1999).

Unit-cell dimensions obtained from XRD and SAED are consistent (Table 2) despite difficulties intrinsic to SAED such as the calibration of the camera constant, the alignment of a single crystal along [001] and the inability to precisely determine α, β and γ angles for a triclinic system. Moreover, the uncertainty on the measured values is low for the two methods (~ 0.1 % and 0.6 % for XRD and SAED, respectively – Table 2). In contrast, a_{or} and b_{or} parameters measured on the talc surface by AFM are scattered and the resulting uncertainty on the unit-cell parameter is much

higher, as discussed above. XRD and SAED (providing a good calibration of the camera constant) are more accurate methods to determine unit-cell parameters because of the improved statistics (for XRD) and of the enhanced sensitivity to crystal geometry.

Because the sample used in the present study presents a quasi-ideal surface structure with extremely limited tetrahedral tilts/rotations and limited surface relaxation, if any, the variation in unit-cell dimensions can, therefore, be attributed to instrumental variability (calibration, tip-sample interaction). Extreme care should thus be used when interpreting the changes in unit-cell dimensions in terms of structural features for other clay minerals such as micas, kaolinites and chlorites in which such structural deformations are likely.

6. Conclusion

In relation with the peculiar crystallinity of the studied talc sample from the Trimouns deposit (Ariège, France), it has been possible, using atomic force microscopy, to obtain a detailed image of the talc surface at the molecular scale. However, in spite of the high-quality image obtained, artefacts that lead to the observation of only one tetrahedron out of two were detected (double-atom cantilever tip interaction). In addition, the very peculiar crystal-chemistry of talc (very limited tetrahedral tilts and tetrahedral rotations, unlikely structure relaxation) has revealed the existence of additional instrumental effects. These effects lead to a slight distortion of the image that make a structural interpretation of these distortions, described in previous studies for other clay minerals (micas, chlorites), ambiguous. Finally the comparison of structure dimensions with data obtained by XRD and SAED highlights the limitations for using AFM for unit-cell dimensions determination because of the increased uncertainty and of the possible distortions (enlargement) by instrumental effects.

References

Abercrombie, H.J., Skippen, G.B., Marshall, D.D. (1987): F-OH substitution in natural tremolite, talc, and phlogopite. *Contrib. Mineral. Petrol.*, **97**, 305-312.

Aldushin, K., Jordan, G., Fechtelkord, M., Schmahl, W.W., Becker, H.W., Rammensee, W. (2004): On the mechanisms of apophyllite alteration in aqueous solutions. A combined AFM, XPS and MAS NMR study. *Clays Clay Minerals*, **52**, 432-442.

Aramu, F., Maxiav, G., Delunas, A. (1989): Mössbauer spectroscopy of talc minerals. *Nuovo Cimento*, **11D**, 891-896.

Bickmore, B.R., Bosbach, D., Hochella, M.F., Charlet, L., Rufe E. (2001): In situ atomic force microscopy study of hectorite and nontronite dissolution: Implications for phyllosilicate edge surface structures and dissolution mechanisms. *Am. Mineral.*, **86**, 411-423.

Blaauw, C., Stroink, G., Leiper, W. (1980): Mössbauer analysis of talc and chlorite. *J. Phys. I*, **41**, 411-412.

Bosbach, D., Charlet, L., Bickmore, B.R., Hochella, M.F.J. (2000): The dissolution of hectorite: *In-situ*, real-time observations using Atomic Force Microscopy. *Am. Mineral.*, **85**, 1209-1216.

Brandt, F., Bosbach, D., Krawczyk-Barsch, E., Arnold, T., Bernhard, G. (2003): Chlorite dissolution in the acid pH-range: A combined microscopic and macroscopic approach. *Geochim. Cosmochim. Acta*, **67**, 1451-1461.

Coey, J.M.D., Bakas, T., Guggenheim, S. (1991): Mössbauer spectra of minnesotaite and ferrous talc. *Am. Mineral.*, **76**, 1905-1909.

De Parseval, P., Fontan, F., Aigouy, T. (1997): Composition chimique des minéraux de terres rares de Trimouns (Ariège, France). *C.R. Acad. Sci. II*, **234**, 625-630.

De Parseval, P., Fournes, L., Fortuné, J.P., Moine, B., Ferret, J. (1991): Distribution du fer dans les chlorites par spectrométrie Mössbauer (^{57}Fe) : Fe(III) dans les chlorites du gisement de talc-chlorite de Trimouns (Pyrénées, France). *C.R. Acad. Sci. II*, **312**, 1321-1326.

De Parseval, P., Moine, B., Fortuné, J.P., Ferret, J. (1993): Fluid-mineral interactions at the origin of the Trimouns talc and chlorite deposit (Pyrénées, France). *in* "Current Research in Geology Applied to Ore Deposits", P. Fenoll Hach-Ali, J. Torres-Ruiz, F. Gervilla, eds. Univ. of Granada, Granada, 205-209.

Drake, B., Prater, C.B., Weisenhorn, A.L., Gould, S.A.C., Albrecht, T.R., Quate, C.F., Cannell, D.S., Hansma, H.G., Hansma, P.K. (1989): Imaging crystals, polymers, and process in water with atomic force microscope. *Science*, **243**, 1586-1589.

Drake, B. & Hellmann, R. (1991): Atomic force microscopy imaging of the albite (010) surface. *Am. Mineral.*, **76**, 1773-1776.

Dyar, M.D. (1993): Mössbauer spectroscopy of tetrahedral Fe(III) in trioctahedral micas. Discussion. *Am. Mineral.*, **78**, 665-668.

Dyar, M.D. & Burns, R.G. (1986): Mössbauer spectral study of ferruginous one-layer trioctahedral micas. *Am. Mineral.*, **71**, 955-965.

Ferrage, E., Martin, F., Boudet, A., Petit, S., Fourty, G., Jouffret, F., Micoud, P., De Parseval, P., Salvi, S., Saint-Gérard, Y., Buratto, S, Ferret, J., Fortuné, J.P. (2002): Talc as nucleating agent of polypropylene : morphology induced by lamellar particles addition and interface mineral-matrix modelisation. *J. Mater. Sci.*, **37**, 1561-1573.

Fortuné, J.P., Gavoille, B., Thiebaut, J. (1980): Le gisement de talc de Trimouns près de Luzenac (Ariège). Publ. 26th Int. Geol. Congr., Issue E10, 43 p.

Gould, S.A.C., Burke, K., Hansma, P.K. (1989): Simple theory for the atomic force microscope with a comparison of theoretical and experimental images of graphite. *Phys. Rev. B*, **40**, 5363-5366.

Gruner, J.W. (1934): The crystal structure of talc and pyrophyllite. *Z. Kristallogr. Krist.*, **88**, 412-419.

Hartman, H., Sposito, G., Yang, A., Manne, S., Gould, S.A.C., Hansma, P.K. (1990): Molecular scale imaging of clay mineral surfaces with the atomic force microscope. *Clays Clay Minerals*, **38**, 337-342.

Heller-Kallai, L. & Rozenson, I. (1981): The use of Mössbauer spectroscopy of iron in clay mineralogy. *Phys. Chem. Minerals*, **7**, 223-238.

Hillner, P.E., Gratz, A.J., Hansma, P.K. (1992a): Composite spiral growth kinetics of calcite revealed by AFM. *Proc. Soc. Photo-Opt. Instrum. Eng.*, **1639**, 160-170.

Hillner, P.E., Manne, S., Hansma, P.K. (1992b): Atomic-scale imaging of calcite growth and dissolution in real time. *Geology*, **20**, 359-362.

Johnsson, P.A., Eggleston, C.M., Hotchella, M.F. Jr. (1991): Imaging molecular-scale structure and microtopography of hematite with the atomic force microscope. *Am. Mineral.*, **76**, 1442-1445.

Kuwahara, Y. (1999): Muscovite surface structure imaged by fluid contact mode AFM. *Phys. Chem. Minerals*, **26**, 198-205.

— (2001): Comparison of the surface structure of tetrahedral sheets of muscovite and phlogopite by AFM. *Phys. Chem. Minerals*, **28**, 1-8.

Kuwahara, Y., Uehara, S., Aoki, Y. (1998): Surface microtopography of lath-shaped hydrothermal illite by tapping-mode and contact-mode AFM. *Clays Clay Minerals*, **46**, 574-582.

—,—,— (2001): Atomic force microscopy study of hydrothermal illite in Izumiyama pottery stone from Arita, Saga Prefecture, Japan. *Clays Clay Minerals*, **49**, 300-309.

Lindgreen, H. (2000): Electrical conduction in layer silicates investigated by combined scanning tunnelling microscopy and atomic force microscopy. *Clay Minerals*, **35**, 643-652.

Lindgreen, H., Garnæs, J., Hansen, P.L., Besenbacher, F., Lægsgaard, E., Stensgaard, I., Gould, S.A., Hansma, P.K. (1991): Ultrafine particles of North Sea illite/smectite clay minerals investigated by STM and AFM. *Am. Mineral.*, **76**, 1218-1222.

Martin, F., Ildefonse, P., Hazemann, J.L., Grauby, O., Decarreau, A. (1996): Random distribution of Ge and Si in synthetic talc: an EXAFS and FTIR study. *Eur. J. Mineral.*, **8**, 289-299.

Martin, F., Micoud, P., Delmotte, L., Marechal, C., Le Dred, R., De Parseval, P., Mari, A., Fortuné, J.P., Salvi, S., Béziat, D., Grauby, O., Ferret, J. (1999): The structural formula of talc from the Trimouns deposit, Pyrénées, France. *Can. Mineral.*, **37**, 975-984.

Moine, B., Gavoille, B., Thiébault, J. (1982): Géochimie des transformations à l'origine du gisement de talc et chlorite de Trimouns (Luzenac, Ariège, France). I - Mobilité des éléments et zonalités. *Bull. Minéral.*, **105**, 62-75.

Moine, B., Fortuné, J.P., Moreau, P., Viguier, F. (1989): Comparative mineralogy, geochemistry and conditions of formation of two metasomatic talc and chlorite deposits : Trimouns (Pyrénées, France) and Rabenwald (Eastern Alps, Austria). *Econ. Geol.*, **84**, 1398-1416.

Noack, Y., Decarreau, A., Manceau, A. (1986): Spectroscopic and oxygen isotopic evidence for low and high temperature origin of talc. *Bull. Minéral.*, **109**, 253-263.

Perdikatsis, B. & Burzlaff, H. (1981): Strukturverfeinerung am Talk $Mg_3Si_4O_{10}(OH)_2$. *Z. Kristallogr.*, **156**, 177-186.

Radoslovitch, E.W. (1961): Surface symmetry and cell dimensions of layer lattice silicates. *Nature*, **191**, 67-68.

— (1962): The cell dimensions and symmetry of layer lattice silicates. I. Some structural considerations. II. Regression relations. *Am. Mineral.*, **47**, 599-636.

Rancourt, D.G. (1993): Mössbauer spectroscopy of tetrahedral Fe(III) in trioctahedral micas. Reply. *Am. Mineral.*, **78**, 669-671.

— (1994): I. Inadequency of lorentzian-line doublets in fitting spectra arising from quadrupole splitting distributions. *Am. Mineral.*, **21**, 244-249.

Rancourt, D.G., Dang, M.Z., Lalonde, A.E. (1992): Mössbauer spectroscopy of tetrahedral Fe(III) in trioctahedral micas. *Am. Mineral.*, **77**, 34-43.

Rayner, J.H. & Brown, G. (1973): The crystal structure of talc. *Clays Clay Minerals*, **21**, 103-114.

Sokolov, I.Y., Henderson, G.S., Wicks, F.J., Ozin, G.A. (1997): Improved atomic force microscopy resolution using an electric double layer. *Appl. Phys. Lett.*, **70**, 844-846.

Sokolov, I.Y., Henderson, G.S., Wicks, F.J. (1999): Theoretical and experimental evidence of "true" atomic resolution under non-vacuum conditions. *J. Appl. Phys.*, **86**, 5537-5540.

Tournassat, C., Neaman, A., Villiéras, F., Bosbach, D., Charlet, L. (2003): Nanomorphology of montmorillonite particles: Estimation of the clay edge sorption site density by low-pressure gas adsorption and AFM observations. *Am. Mineral.*, **88**, 1989-1995.

Vrdoljak, G.A., Henderson, G.S., Fawcett, J.J., Wicks, F.J. (1994): Structural relaxation of the chlorite surface imaged by the atomic force microscope. *Am. Mineral.*, **79**, 107-112.

Weisenhorn, A.L., Mac Dougell, J.E., Gould, Cox, S.A.C., Cox, S.D., Wise, W.S., Massie, J., Maivald, P., Elings, V.B., Stucky, G.D., Hansma, P.K. (1990): Imaging and Manipulating Molecules on a Zeolite Surface with an Atomic Force Microscope. *Science*, **247**, 1330-1333.

Wicks, F.J., Kjoller, K., Henderson, G.S. (1992): Imaging the hydroxyl surface of lizardite at atomic resolution with the atomic force microscope. *Can. Mineral.*, **30**, 83-91.

Wicks, F.J., Kjoller, K., Eby, R.K., Hawthorne, F.C., Henderson, G.S., Vrdoljak, G.A. (1993): Imaging the internal atomic structure of layer silicates using the atomic force microscope. *Can. Mineral.*, **31**, 541-550.

Wicks, F.J., Henderson, G.S., Hawthorne, F.C., Kjoller, K. (1998): Evidence for atomic-scale resolution in atomic force microscopy of layer silicates. *Can. Mineral.*, **36**, 1607-1614.

Yokoyama, S., Kuroda, M., Sato, T. (2005): Atomic force microscopy study of montmorillonite dissolution under highly alkaline conditions. *Clays Clay Minerals*, **53**, 147-154.